Narrow-Band Measurement of Differential Group Delay by a Six-State RF Phase-Shift Technique: 40 fs Single-Measurement Uncertainty

P. A. Williams and J. D. Kofler

Abstract—**We describe in detail our implementation of a modulation phase shift (MPS) technique for narrow-bandwidth measurement of differential group delay (DGD) and the principal states of polarization (PSP) in optical fibers and components. Our MPS technique involves launching six orthogonal polarization states (as opposed to the four states typically launched) to achieve improved measurement stability. The measurement bandwidth is 4.92 GHz (twice the 2.46 GHz RF modulation frequency), the measurement time is 13 s per point, and the single-measurement uncertainty is better than 40 fs (~95% confidence interval) for DGD values from 10 to 1000 fs. We demonstrate that this uncertainty can be greatly improved by averaging, yielding a 9.7 fs uncertainty (95% confidence interval) on a device with 315 fs of DGD. Sources of uncertainty are detailed, including a DGD contribution from the detector itself. Simulations illustrate the uncertainty contribution of multiple DGD elements in series.**

Index Terms—**Differential group delay (DGD), modulation phase shift (MPS), polarization-mode dispersion (PMD), RF phase shift.**

I. Introduction

POLARIZATION-MODE DISPERSION (PMD) in optical fibers or components is a polarization-dependent propagation delay, measured as the differential group delay (DGD) between the fastest and slowest propagation modes. PMD results in pulse distortion and increased bit error rates in optical communications systems, so it must be well characterized. Fundamentally, a finite bandwidth is required to measure group delay, resulting in a tradeoff between frequency resolution and DGD measurement uncertainty. In recent years, techniques have been developed to efficiently measure DGD in a narrow spectral bandwidth. The two major approaches are RF phase-shift based approaches [1], [2], and swept-wavelength interferometry [3]. Here we describe the specific implementation of our modulation phase shift (MPS) system for simultaneous measurement of DGD and the principal states of polarization (PSP). Since optimum performance of the MPS system requires careful system design [4], we also detail the uncertainty analysis of the measurement system. We validate measurement results by comparison with artifacts measured using the technique of Jones matrix eigenanalysis (JME) [5].

Manuscript received July 24, 2003; revised September 16, 2003.

The authors are with the National Institute of Standards and Technology, Boulder, CO 80305 USA (e-mail: paul.williams@nist.gov).

Digital Object Identifier 10.1109/JLT.2003.822116

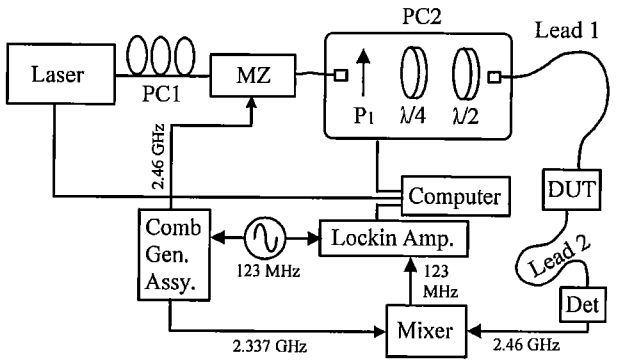

Fig. 1. Schematic diagram of modulation phase shift measurement system. PC1 and PC2 are polarization controllers, MZ is a Mach–Zehnder intensity modulator, P1 is a Glan-Thompson polarizer, $\lambda/4$ and $\lambda/2$ are quarter- and half-wave plates, DUT is the device under test, and Det is the detector. Comb Gen. Assy. is the comb generator assembly, detailed in Fig. 3.

II. Measurement Description

The measurement setup is as shown schematically in Fig. 1. The idea is to launch known polarization states of RF-modulated light into the device under test (DUT) and measure the resulting radio-frequency (RF) phase of the light at the detector. Since RF phase at the detector depends on the group delay through the device under test, varying the launched polarization state will allow the polarization-dependent group delay through the device to be measured. This yields the DGD and the PSP.

Specifically, this is done as follows. A tunable laser is amplitude modulated at 2.46 GHz by means of a Mach–Zehnder modulator (passively biased at quadrature). The polarization state of the light is deterministically controlled by the polarization controller (PC2). The light is then input into the DUT. At the exit of the DUT, the light is detected with a 7-GHz bandwidth detector. Using a lock-in amplifier, the RF phase of the detected signal is compared with that of the RF signal driving the modulator. The measured RF phase for four mutually orthogonal polarization states is sufficient to determine both the DGD and the PSP [1], [2]. However, to reduce measurement noise, we perform the measurement by launching a set of six mutually orthogonal polarization states.[1] The absolute orientation of these six states has no bearing on the measured DGD (provided they maintain their mutually orthogonal relationship with each other), but defines the basis vector set (in Stokes space) with which the direction of the polarization dispersion vector (PDV) is defined. As will

[1]"Six mutually orthogonal polarization states" refers to four states evenly spaced on a great circle of the Poincaré sphere and two states defined by the axis of that circle.

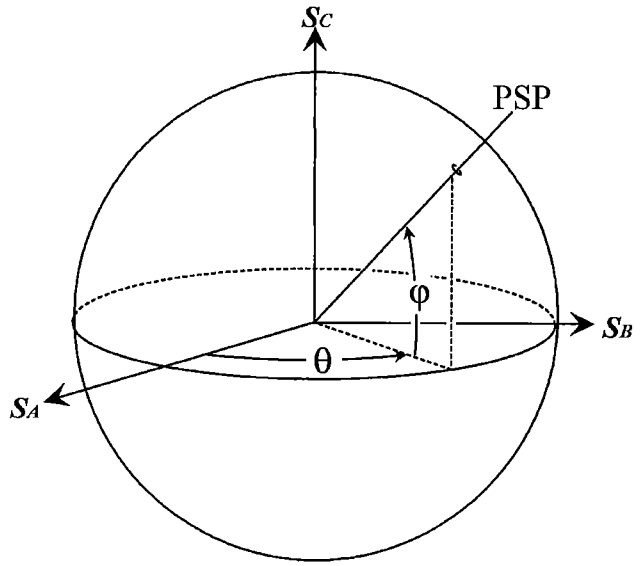

Fig. 2. Poincaré sphere representation of three general states $\boldsymbol{S_A}$, $\boldsymbol{S_B}$, and $\boldsymbol{S_C}$, chosen to be mutually orthogonal. φ and θ define the position of the principal state of polarization (PSP) in terms of the $\boldsymbol{S_A}$, $\boldsymbol{S_B}$, and $\boldsymbol{S_C}$, axes.

be explained later, we perform averaging by randomizing the offset orientation of the six-state sets being launched but transform the measured PDV so that its definition is independent of the absolute orientation of the launched states.

The details of this six-state launch technique follow closely those of the four-state launch, described in [1]. For an arbitrary input polarization state whose Stokes vector makes an angle of α (in Poincaré sphere coordinates) with the PSP of the device under test, the RF phase delay of the transmitted light is given as

$$\phi_{\mathrm{RF}} = \tan^{-1}(\cos\alpha \tan \Delta\tau\pi f) + \Phi \tag{1}$$

where $\Delta\tau$ is the DGD of the DUT, f is the RF modulation frequency, and Φ is the polarization-independent phase delay. With complete generality, we consider three mutually orthogonal polarization state vectors $\boldsymbol{S_A}$, $\boldsymbol{S_B}$, and $\boldsymbol{S_C}$, ($\boldsymbol{S_A}\cdot\boldsymbol{S_B} = \boldsymbol{S_A}\cdot\boldsymbol{S_C} = \boldsymbol{S_B}\cdot\boldsymbol{S_C} = 0$) shown in Fig. 2. Following the work of [1], we find that light launched with the polarization states $\mathbf{S_A}$, $\mathbf{S_B}$, and $\mathbf{S_C}$ arrives with the following RF phases (respectively)

$$\phi_{\mathrm{RF},S_A} = \tan^{-1}(\cos\varphi \sin\theta \tan \Delta\tau\pi f) + \Phi \tag{2}$$

$$\phi_{\mathrm{RF},S_B} = \tan^{-1}(\cos\varphi \sin\theta \tan \Delta\tau\pi f) + \Phi \tag{3}$$

and

$$\phi_{\mathrm{RF},S_C} = \tan^{-1}(\sin\varphi \tan \Delta\tau\pi f) + \Phi. \tag{4}$$

φ is the elevation angle of the PSP, and θ is its azimuth, measured with respect to $\mathbf{S_A}$, $\mathbf{S_B}$, and $\mathbf{S_C}$ (Fig. 2). For light launched on the opposite side of the Poincaré sphere, along $-\mathbf{S_A}$, $-\mathbf{S_B}$, and $-\mathbf{S_C}$, we would measure the following phases

$$\phi_{\mathrm{RF},-S_A} = -\tan^{-1}(\cos\varphi \sin\theta \tan \Delta\tau\pi f) + \Phi \tag{5}$$

$$\phi_{\mathrm{RF},-S_B} = -\tan^{-1}(\cos\varphi \sin\theta \tan \Delta\tau\pi f) + \Phi \tag{6}$$

and

$$\phi_{\mathrm{RF},-S_C} = -\tan^{-1}(\sin\varphi \tan \Delta\tau\pi f) + \Phi. \tag{7}$$

Assuming these opposite pairs experience the same polarization-independent phase, we find that the differences

$$\Delta\phi_{\mathrm{RF},S_A} = \frac{(\phi_{\mathrm{RF},S_A} - \phi_{\mathrm{RF},-S_A})}{2} \tag{8}$$

$$\Delta\phi_{\mathrm{RF},S_B} = \frac{(\phi_{\mathrm{RF},S_B} - \phi_{\mathrm{RF},-S_B})}{2} \tag{9}$$

and

$$\Delta\phi_{\mathrm{RF},S_C} = \frac{(\phi_{\mathrm{RF},S_C} - \phi_{\mathrm{RF},-S_C})}{2} \tag{10}$$

each eliminate Φ and yield only the polarization-dependent portions of the RF phase.

However, Φ is the polarization-independent accumulated phase from the full optical path length of the device and its value can drift significantly with environmental conditions as well as fiber motion. To minimize the effect of this drift during a measurement, we launch the six states in such an order that antiparallel states are launched sequentially and in groups of three. For example, states $\boldsymbol{S_A}$, $-\boldsymbol{S_A}$, and $\boldsymbol{S_A}$ are launched and their respective measured RF phases are ϕ_{RF,S_A1}, $\phi_{\mathrm{RF},-S_A}$, and ϕ_{RF,S_A2}. Measuring three states like this takes about 4.3 s. If Φ drifts in that time, then ϕ_{RF,S_A1} will differ from ϕ_{RF,S_A2}, so we use their average $\phi_{\mathrm{RF},S_A} = (\phi_{\mathrm{RF},S_A1} + \phi_{\mathrm{RF},S_A2})/2$ to calculate $\Delta\phi_{\mathrm{RF},S_A}$ in (8). This is repeated for the $\boldsymbol{S_B}$ and $\boldsymbol{S_C}$ states. This eliminates errors due to group delay drift as long as Φ changes linearly over the 4.3 s sampling period. We further attempt to mitigate the effects of Φ drift by changing the order in which $\boldsymbol{S_A}$, $\boldsymbol{S_B}$, and $\boldsymbol{S_C}$ are launched. For one data point, the full measurement order may be $\boldsymbol{S_A}$, $-\boldsymbol{S_A}$, $\boldsymbol{S_A}$, $\boldsymbol{S_B}$, $-\boldsymbol{S_B}$, $\boldsymbol{S_B}$, $\boldsymbol{S_C}$, $-\boldsymbol{S_C}$, $\boldsymbol{S_C}$, and for the next data point, the order might be $\boldsymbol{S_B}$, $-\boldsymbol{S_B}$, $\boldsymbol{S_B}$, $\boldsymbol{S_A}$, $-\boldsymbol{S_A}$, $\boldsymbol{S_A}$, $\boldsymbol{S_C}$, $-\boldsymbol{S_C}$, $\boldsymbol{S_C}$, etc. This randomizes any bias in the DGD measurements due to drift that is not yet compensated.

Combining (2) through (10), we get (11) found at the bottom of the page. Here, we find that (11) yields the DGD of the device under test. Note that due to sign ambiguities, this is not a general definition but is completely correct as it is used here. This expression, based on a six-state launch, is more robust against phase drift than the four-state launch of [1]. This is because we require Φ to be stable only over one-third of the full 13-s measurement time; the four-state launch requires phase stability for the entire measurement time. This difference may seem minor, but we see a significant improvement in the noise floor when using the six-state technique. The argument might be made that

$$\Delta\tau = \frac{\tan^{-1}\left\{\sqrt{\tan^2\Delta\phi_{\mathrm{RF},S_A} + \tan^2\Delta\phi_{\mathrm{RF},S_B} + \tan^2\Delta\phi_{\mathrm{RF},S_C}}\right\}}{\pi f} \tag{11}$$

the six-state technique improves the measurement merely by a greater number of measurements. While more measurements allow reduction of random noise effects, the real advantage of the six-state technique over the four-state approach is the reduced time between measurements of Φ, which significantly improves the system's immunity to group delay drift (which cannot be eliminated by merely measuring more data points).

These six RF phases can be used to yield not only the magnitude of the DGD, but its vector direction as well. The PDV gives the full vector description of the PMD; it is a vector in Stokes space that points along the fast PSP of the device and whose magnitude is the DGD. Equation (1) illustrates how the arrival phase for a given launched polarization state depends on the projection of the launched polarization state onto the PSP. If $\boldsymbol{p}$ denotes a unit vector pointing in the direction of the fast PSP, then $\cos(\alpha)$ in (1) is the dot product of the launched polarization state and $\boldsymbol{p}$, and α becomes the angle between the PSP fast axis and the particular launched state. For the launch states $\boldsymbol{S_A}$, $\boldsymbol{S_B}$, and $\boldsymbol{S_C}$, we denote the corresponding α values as

$$\begin{aligned}\cos(\alpha_A) &= \boldsymbol{p}\cdot\boldsymbol{S_A},\\ \cos(\alpha_B) &= \boldsymbol{p}\cdot\boldsymbol{S_B},\\ \cos(\alpha_C) &= \boldsymbol{p}\cdot\boldsymbol{S_C}.\end{aligned} \tag{12}$$

We find these projections by using (2) through (10)

$$\cos(\alpha_A) = \frac{\tan\left(\Delta\phi_{=\mathrm{RF},S_A}\right)}{\tan(\Delta\tau\pi f)} \tag{13}$$

$$\cos(\alpha_B) = \frac{\tan\left(\Delta\phi_{\mathrm{RF},S_B}\right)}{\tan(\Delta\tau\pi f)} \tag{14}$$

and

$$\cos(\alpha_C) = \frac{\tan\left(\Delta\phi_{\mathrm{RF},S_C}\right)}{\tan(\Delta\tau\pi f)}. \tag{15}$$

So (13) through (15) describe the direction cosines of the PSP vector in terms of the basis defined by $\boldsymbol{S_A}$, $\boldsymbol{S_B}$, and $\boldsymbol{S_C}$. As an initial simplification, we consider the case where $\boldsymbol{S_A}$, $\boldsymbol{S_B}$, and $\boldsymbol{S_C}$ are, respectively, linear horizontal, linear 45°, and right-hand circularly polarized light, denoted by the standard Stokes vectors (in reduced notation) as $\boldsymbol{S}_1 = (1,0,0)^{\mathrm{T}}$, $\boldsymbol{S}_2 = (0,1,0)^{\mathrm{T}}$, and $\boldsymbol{S}_3 = (0,0,1)^{\mathrm{T}}$, where the superscript "T" denotes the transpose. Then, the direction cosines will yield the reduced-notation Stokes vector of the PSP

$$\boldsymbol{p} = \frac{1}{\tan(\Delta\tau\pi f)}\begin{pmatrix}\tan\left(\Delta\phi_{\mathrm{RF},S_1}\right)\\ \tan\left(\Delta\phi_{\mathrm{RF},S_2}\right)\\ \tan\left(\Delta\phi_{\mathrm{RF},S_3}\right)\end{pmatrix} \tag{16}$$

and, the full vector PMD is described by the PDV (denoted $\boldsymbol{\Omega}$)

$$\boldsymbol{\Omega} = \Delta\tau\boldsymbol{p} = \frac{\Delta\tau}{\tan(\Delta\tau\pi f)}\begin{pmatrix}\tan\left(\Delta\phi_{\mathrm{RF},S_1}\right)\\ \tan\left(\Delta\phi_{\mathrm{RF},S_2}\right)\\ \tan\left(\Delta\phi_{\mathrm{RF},S_3}\right)\end{pmatrix}. \tag{17}$$

Experimentally, we find that randomizing the absolute orientation of the six-state launched set minimizes the effects of internal DGD in the polarization controller. We describe the orientation of the launched set in Stokes space by selecting a random set of Euler angles β, γ, and ψ [6]. From these we generate the general transfer matrix (see (18), shown at the bottom of the page) to rotate an orthogonal six-state set to an arbitrary orientation.

We describe the general set of mutually orthogonal launch states $\boldsymbol{S_A}$, $\boldsymbol{S_B}$, and $\boldsymbol{S_C}$ in terms of these Euler rotations of the reduced Stokes vectors as

$$\begin{aligned}\boldsymbol{S_A}(\beta,\gamma,\psi) &= \boldsymbol{A}(\beta,\gamma,\psi)\boldsymbol{S}_1\\ \boldsymbol{S_B}(\beta,\gamma,\psi) &= \boldsymbol{A}(\beta,\gamma,\psi)\boldsymbol{S}_2\\ \boldsymbol{S_C}(\beta,\gamma,\psi) &= \boldsymbol{A}(\beta,\gamma,\psi)\boldsymbol{S}_3.\end{aligned} \tag{19}$$

So, $\boldsymbol{S_A}$, $\boldsymbol{S_B}$, and $\boldsymbol{S_C}$ can be defined by their Euler angles β, γ, and ψ, and are expressed in Stokes space as

$$\begin{aligned}\boldsymbol{S_A} &= \begin{pmatrix}\cos\psi\cos\beta - \cos\gamma\sin\beta\sin\psi\\ -\sin\psi\cos\beta - \cos\gamma\sin\beta\cos\psi\\ \sin\gamma\sin\beta\end{pmatrix},\\ \boldsymbol{S_B} &= \begin{pmatrix}\cos\psi\sin\beta + \cos\gamma\cos\beta\sin\psi\\ -\sin\psi\sin\beta + \cos\gamma\cos\beta\cos\psi\\ -\sin\gamma\cos\beta\end{pmatrix},\\ \boldsymbol{S_C} &= \begin{pmatrix}\sin\psi\sin\gamma\\ \cos\psi\sin\gamma\\ \cos\gamma\end{pmatrix}.\end{aligned} \tag{20}$$

The DGD calculated from (11) is independent of the absolute orientation of the six-state set. So launching the polarization states defined by (20) yields the DGD, regardless of the choice of β, γ, and ψ. However, to describe the direction of the PMD vector requires knowledge of the absolute orientation of the launched states. The quantity

$$\boldsymbol{p}_{ABC} = \frac{1}{\tan(\Delta\tau\pi f)}\begin{pmatrix}\tan\left(\Delta\phi_{\mathrm{RF},S_A}\right)\\ \tan\left(\Delta\phi_{\mathrm{RF},S_B}\right)\\ \tan\left(\Delta\phi_{\mathrm{RF},S_C}\right)\end{pmatrix} \tag{21}$$

is the PSP expressed in a basis set defined by the axes $\boldsymbol{S_A}$, $\boldsymbol{S_B}$, and $\boldsymbol{S_C}$. We find the PSP in the Stokes space basis by undoing the vector transformation, so that

$$\boldsymbol{p} = \boldsymbol{A}(-\psi,-\gamma,-\beta)\boldsymbol{p}_{ABC}. \tag{22}$$

In other words, when we launch an arbitrary six-state orthogonal polarization set $\boldsymbol{S_A}$, $-\boldsymbol{S_A}$, $\boldsymbol{S_B}$, $-\boldsymbol{S_B}$, $\boldsymbol{S_C}$, and $-\boldsymbol{S_C}$, the PSP is given (in a Stokes-space basis) as

$$\boldsymbol{p} = \frac{1}{\tan(\Delta\tau\pi f)}\boldsymbol{A}(-\psi,-\gamma,-\beta)\begin{pmatrix}\tan\left(\Delta\phi_{\mathrm{RF},S_A}\right)\\ \tan\left(\Delta\phi_{\mathrm{RF},S_B}\right)\\ \tan\left(\Delta\phi_{\mathrm{RF},S_C}\right)\end{pmatrix} \tag{23}$$

$$\boldsymbol{A}(\beta,\gamma,\psi) = \begin{pmatrix}\cos\psi\cos\beta - \cos\gamma\sin\beta\sin\psi & \cos\psi\sin\beta + \cos\gamma\cos\beta\sin\psi & \sin\psi\sin\gamma\\ -\sin\psi\cos\beta - \cos\gamma\sin\beta\cos\psi & -\sin\psi\sin\beta + \cos\gamma\cos\beta\cos\psi & \cos\psi\sin\gamma\\ \sin\gamma\sin\beta & -\sin\gamma\cos\beta & \cos\gamma\end{pmatrix}. \tag{18}$$

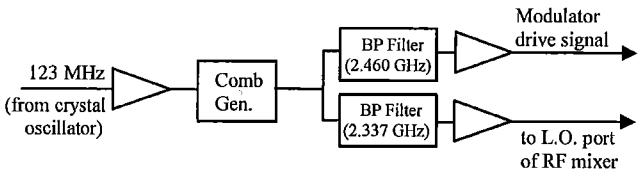

Fig. 3. Comb Generator Assembly. Schematic of RF electronics used to generate 2.337 and 2.46 GHz signals and then to mix back down to 123 MHz, which is readable with the lock-in amplifier. BP Filter is a bandpass filter.

and the full polarization dispersion vector is given by

$$\mathbf{\Omega} = \frac{\Delta\tau}{\tan(\Delta\tau\pi f)}\boldsymbol{A}(-\psi,-\gamma,-\beta)\begin{pmatrix}\tan\left(\Delta\phi_{\mathrm{RF},S_A}\right)\\ \tan\left(\Delta\phi_{\mathrm{RF},S_B}\right)\\ \tan\left(\Delta\phi_{\mathrm{RF},S_C}\right)\end{pmatrix}. \tag{24}$$

We use (11) and (24) to calculate the full vector PDV.

A. DGD Measurement (Experimental Details)

1) Measurement Range: The minimum DGD measurable with this MPS system is determined by the noise floor. As seen from the uncertainty analysis that follows, when the DGD of the DUT is below about 10 fs, the bias due to internal DGD (polarization-dependent group delay internal to our measurement system) begins to dominate. So we use 10 fs as the practical lower measurement limit. The upper limit is determined by a 180° phase ambiguity at the lock-in amplifier. The difference in RF phase at the lock-in $\Delta\varphi$ (in degrees) between two launched polarization states is related to their group delay difference and RF modulation frequency as

$$\Delta\tau = \frac{\Delta\varphi}{360\cdot f}. \tag{25}$$

So to avoid a 180° ambiguity in phase, the largest DGD that could be measured is $1/(2f)$. For $f = 2.46$ GHz, the maximum measurable DGD is 203 ps.

2) RF Electronics: The measurement system is based on an RF lock-in amplifier (200 MHz bandwidth) with a phase resolution of 0.02°. In order to increase the temporal sensitivity of the system, we operate our modulator at 2.46 GHz and mix the signal down to 123 MHz so that the phase can be read by the lock-in amplifier. Fig. 3 illustrates this process schematically. The output of an oven-controlled crystal oscillator at 123 MHz is amplified to approximately 0.5 W and sent to a comb generator. The comb generator produces harmonics of the fundamental 123 MHz signal. Using cavity filters, the harmonic at 2.460 GHz is selected and amplified for use in driving the Mach–Zehnder modulator, and the adjacent harmonic at 2.337 GHz is selected and fed to the local-oscillator (LO) port of the mixer. The 2.460 GHz signal received from the optical detector is fed into the RF port of the mixer and the intermediate-frequency (IF) output from the mixer is at the frequency difference (123 MHz) between the two, but retains the phase information from the 2.460 GHz detected signal. This IF signal is amplified and sent to the "signal" side of the lock-in amplifier. In principle, a $\Delta\varphi = 0.02°$ phase resolution at the lock-in amplifier and a $f = 2.460$ GHz modulation frequency allows a temporal resolution of

$$\delta t = \frac{\Delta\varphi}{360\cdot f} = \frac{0.02}{360\cdot 2.46\times 10^9\ s^{-1}} = 22.6\ \text{fs}. \tag{26}$$

In practice, the achievable resolution can be limited by other sources of noise as well. The achievable phase noise is described in the uncertainty analysis section of this paper.

To obtain the best performance, we took care in assembling this comb-generator/mixer section to assure that it did not add phase noise. We selected amplifier components based on low noise-figure specifications. When the system was assembled, we monitored the stability of the phase reading on the lock-in amplifier. Once the system was warmed up for a couple of hours, we observed phase variations of only one or two hundredths of a degree over a couple of seconds. This indicated that we had achieved a setup where the lock-in amplifier or drift in the DUT was the limiting factor to the phase noise. If the phase showed more noise than this, it usually indicated reflections occurring in the system (either optically or electrically) or coherent pickup in the detector. Carefully cleaning each RF and optical connector and using a torque wrench to make the RF connections at the proper tightness reduced the possibility of reflections. Wrapping the detector in aluminum foil reduced the coherent pickup to below −50 dB.

3) Measurement Technique: We found DGD internal to our MPS measurement system. The polarization controller, the fiber leads, and the detector all have inherent DGD, which could bias measurement results. The value of the internal DGD in each of these components and its measurement is detailed in Appendix A. Given the uncertainty due to these internal sources of DGD, we find that the MPS system makes its most accurate measurements when the fiber leads between the polarization controller and the DUT and the leads between the DUT and the detector are reoriented between measurements and the results are averaged. The justification and details are given in Appendix B. In short, this randomizes the alignment of the various DGD elements, and the resulting average DGD of multiple measurements yields a minimum uncertainty due to internal DGD in the measurement system.

So when lower uncertainty is important, the DGD is measured as the average of multiple measurements made with the fiber leads ("Lead 1" and "Lead 2" of Fig. 1) repositioned between each measurement. We find that we get the best averaging for lead lengths of 1 m since this permits sufficient randomization of the polarization state between devices without introducing too much DGD from the leads themselves.

III. Uncertainty Analysis

In assigning an uncertainty to our MPS measurement system, we quantify the sources of uncertainty, and determine how they scale with multiple measurements.

A. Sources of Uncertainty

1) Stokes Noise on Launched Polarization States: The six "mutually orthogonal" launched polarization states require no

particular absolute orientation, but their relative orientation with respect to each other is important. Through simulation, we find that a 3° standard deviation on the launched polarization states yields a 1% noise on the measured DGD. Since our polarization controller (PC2) has an angular repeatability of waveplate rotation of approximately 0.1°, random Stokes noise on the launched states is not a significant error source. However, we do correct the rotation settings of the quarter- and half-waveplate for wavelength changes.

2) Internal DGD: As described in Appendix A, four elements inside our MPS system have measurable DGD. These elements and their effective DGDs are: the polarization controller (PC2 in Fig. 1), 9 fs; upstream fiber "Lead 1," 0.8 fs; downstream fiber "Lead 2," 0.8 fs; and detector, 11 fs. As aforementioned, the effects of these internal DGD sources can be minimized by multiple measurements with the fiber leads reoriented, though averaging the DGD measured for multiple orientations of the fiber leads cannot completely remove the effects of internal DGD. However, Appendix B shows that when the DGD of the DUT is reasonably larger than the inherent DGD in the measurement system, multiple averages can quickly reduce the measurement error to negligible amounts. Fig. 7 gives the expected bias and standard deviation as a function of DUT value. As described, the standard deviation of the mean for multiple measurements scales as $N_F^{-1/2}$, where N_F is the number of statistically independent measurements (i.e., those measured with the fiber leads reoriented between measurements).

In a single measurement, internal DGD contributes a DGD bias $\Delta\tau_{\rm Int}$ and a random DGD error $\sigma_{\rm Int}$, both of which depend on the DGD of the DUT. The bias due to internal DGD does not reduce with multiple measurements, but the random portion of the internal DGD uncertainty does. The total uncertainty contribution due to internal DGD will be

$$u_{\rm Int} = \Delta\tau_{\rm Int} + \frac{\sigma_{\rm Int}}{\sqrt{N_F}} \tag{27}$$

where, as aforementioned, both $\Delta\tau_{\rm Int}$ and $\sigma_{\rm Int}$ depend weakly on the DGD of the DUT. For practical applications where the DGD of the DUT ($\Delta\tau_{\rm DUT}$) is over 10 fs, we can approximate (B2) to find

$$\Delta\tau_{\rm Int} \approx \frac{79.4\ {\rm fs}^2}{\Delta\tau_{\rm DUT}} \tag{28}$$

where $\Delta\tau_{\rm DUT}$ and $\Delta\tau_{\rm Int}$ are in units of femtoseconds. From Fig. 7, we approximate $\sigma_{\rm Int} \approx 8.3$ fs.

3) Phase Noise: Besides internal DGD, another source of measurement uncertainty is RF phase noise. Phase noise can occur due to electrical noise in the measurement system, RF pick-up at the detector, multiple reflections in either the optical or the electrical signal path, and temperature-induced changes in the optical path length. As aforementioned, we minimize phase noise due to electrical effects by cleaning and shielding. If there is an optical cavity in the system, it can cause multiple reflections, which show up as spectral ripple on the measured DGD [7], [8]. Cavities within the measurement system itself have been eliminated (usually by cleaning optical connections). However, if cavities exist within the DUT, the resulting DGD spectral ripple is a real feature of the DUT and should be carefully measured.

With optical reflections minimized, the phase noise that remains is seen as a variation with time of the measured RF phase. We characterize this noise as the standard deviation of the measured DGD for repeated measurements (without moving the leads) of a DUT with a fixed DGD value. We find this standard deviation $\sigma_{\rm phase}$ to be 8.9 fs when measuring a device with 315 fs of DGD. It should be noted that this phase noise can be averaged through multiple measurements. The fiber leads do not need to be reoriented during these averages (in contrast to the case of internal DGD). The uncertainty due to phase noise is expressed as

$$u_{\rm phase} = \frac{\sigma_{\rm phase}}{\sqrt{N_{\rm Tot}}} \tag{29}$$

where $N_{\rm Tot}$ is the total number of measurements made.

4) Frequency Accuracy: Equation (25) relates a change in group delay to a change in RF phase and RF modulation frequency. Therefore, the uncertainty in differential group delay will be affected by the uncertainty in RF frequency f. However, this is a negligible contribution, since f is stable and measurable to at least 5 decimal places.

5) Phase Linearity: Another source of uncertainty is nonlinearity of the phase measurement, that is, a phase error that depends on the magnitude of the phase being measured. To measure the phase nonlinearity, we constructed a PMD emulator from a polarizing Mach–Zehnder interferometer where the polarization state of light in each arm is orthogonal to that in the other arm. Therefore, by changing the length of one of the arms, the DGD of the emulator is changed. Using a distance-measuring interferometer to sense the position of the movable arm allows a high-resolution prediction of the device DGD. Dynamics caused by thermal drift in the emulator limit its uncertainty to 1.5%. Using our MPS system, we measured the DGD of this emulator for DGD values of nominally 175 fs, 315 fs, 1 ps, 50 ps, and 100 ps. We found agreement between the MPS measurement and the predicted value well within the 1.5% accuracy of the emulator. We therefore set the maximum possible nonlinearity of our MPS measurement to this 1.5% level, $\eta = 0.015$. The uncertainty due to this possible nonlinearity is then given as $u_{\rm lin} = \eta\Delta\tau_{\rm DUT}$.

B. Uncertainty Summary

We combine the significant uncertainty sources to give the combined standard uncertainty $u_{\rm Tot}$ of a measurement as the quadrature sum of the uncertainty components

$$u_{\rm Tot} = \sqrt{u_{\rm Int}^2 + u_{\rm phase}^2 + u_{\rm lin}^2} \tag{30}$$

or

$$U = 2u_{\rm Tot} = 2\sqrt{\Delta\tau_{\rm Int}^2 + \left(\frac{\sigma_{\rm Int}}{\sqrt{N_F}}\right)^2 + \left(\frac{\sigma_{\rm phase}}{\sqrt{N_{\rm Tot}}}\right)^2 + (\eta\Delta\tau)^2} \tag{31}$$

where $N_{\rm Tot}$ is the total number of measurements being averaged, N_F is the number of measurements made with the fiber leads reoriented between measurements, and U is the expanded uncertainty [9]. The coverage factor of 2 gives an approximate

TABLE I
DGD UNCERTAINTY COMPONENTS, VALID WHEN DUT DGD IS GREATER THAN 10 fs. $\Delta\tau_{DUT}$ IS IN FEMTOSECONDS

Uncertainty Source	Standard Uncertainty, fs
Internal DGD (bias), $\Delta\tau_{Int}$	$79.4/\Delta\tau_{DUT}$
Internal DGD (random), σ_{Int}	8.3
Phase noise, σ_{phase}	8.9
DGD nonlinearity, $\eta\Delta\tau_{DUT}$	$0.015\Delta\tau_{DUT}$

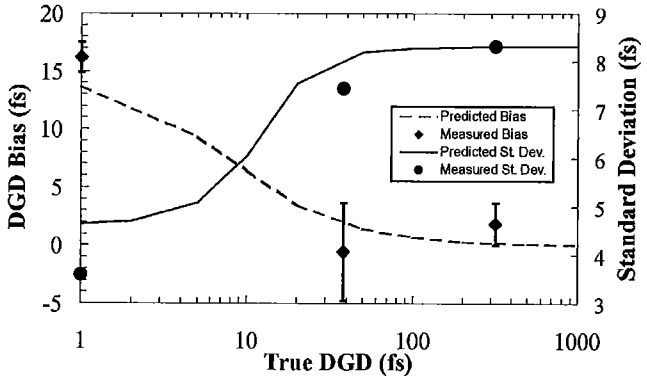

Fig. 4. Measured and theoretical uncertainties as a function of true DGD of the device under test. Error bars represent two standard deviations of the mean for the multiple measurements. Note: the points measured for no DUT were plotted with a predicted DGD value of 1 fs instead of 0. This was done merely to allow plotting on the log scale.

95% confidence interval. We summarize the uncertainty values in Table I.

C. Uncertainty Verification

Since our expanded uncertainty estimate is based on simulation, we made measurements to verify it experimentally. We used a temperature-controlled, pigtailed quartz waveplate with a well-known DGD of nominally 315 fs [10]. We made a total of 1471 measurements over several days, at wavelengths ranging from 1530 nm to 1590 nm, with the fiber leads reoriented for 118 of these measurements to reduce effects of internal DGD. Correcting for known wavelength dependence of the waveplate, we find a 1.9 fs mean discrepancy between our measured mean DGD values and the known values. Using (31) and Table I, with $N_{\mathrm{Tot}} = 1471$ and $N_F = 118$, we find the expanded uncertainty of this measurement to be to be 9.7 fs. So, our 1.9 fs measured error is well within the uncertainty.

We also verified the bias and random uncertainty predictions of Appendix B by measuring three cases: the pigtailed quartz plate artifact described above, a stressed fiber with 38.2 fs of DGD, and the case of no DUT in place at all. In other words, we tested the predictions of Fig. 7 at three points (0, 38.2 fs, and 315 fs). The results are shown in Fig. 4. From our measurements of the pigtailed quartz plate artifact, we measured the bias to be 1.9 fs (as described earlier), and the normalized standard deviation for the 118 independent measurements to be 8.3 fs. The stressed fiber was a 1-m length of standard single-mode fiber that was clamped tightly between two blocks of aluminum (approximately 9 cm long), so that a stress-induced DGD was introduced (measured using the JME technique to be 38.2±4 fs over a 1550–1560 nm wavelength range). We measured the mean DGD of this fiber using the MPS system. We made 10 to 20 measurements evenly spaced over the wavelength range. Then, the fiber leads were rearranged and the measurement repeated. We ended up with 21 independent measurements. The mean MPS-measured DGD was 37.6 fs (a −0.6 fs bias), and we measured a 7.4 fs standard deviation within those 21 measurements. Finally, in measuring the DGD with no DUT in place, we made 20 independent measurements (with the leads moved between measurements)—each of these measurements involved averaging 10–20 repeated measurements made without reorienting the leads. We measured a mean DGD of 16.2 fs with a standard deviation of 3.6 fs. The bias and standard deviation for these three cases are plotted along with the theoretical prediction of Appendix B in Fig. 4. We see reasonable agreement. Error bars on the plot represent two standard deviations of the mean for the multiple measurements.

As a further example of the use of (31) to predict uncertainty, we calculate the predicted uncertainty for measurement of the pigtailed quartz plate device, above, but with no averaging (a single measurement with no fiber lead reorientation). Setting $N_F = N_{\mathrm{Tot}} = 1$, we predict the expanded uncertainty will be 26 fs. We also find that for a DUT with a DGD of 1000 fs, the single-measurement uncertainty will be 37 fs. So, we generalize that for devices with DGD between 10 fs and 1000 fs, the single-measurement random expanded uncertainty will be less than 40 fs, with an approximately 95% confidence interval.

It is useful to compare this level of uncertainty with other measurement techniques. In PMD measurements, there is the inherent tradeoff between temporal uncertainty and frequency resolution of the measurement. An appropriate figure of merit is the bandwidth efficiency factor [11], which measures the normalized signal-to-noise ratio (SNR) achievable per measurement bandwidth. Appendix C calculates the bandwidth efficiency factor for DGD measurements made with this MPS system. We find a bandwidth efficiency factor of approximately 3600. This can be compared with bandwidth efficiency factors of ~800 and ~950 to ~1500 when using JME and swept-wavelength interferometry measurements, respectively. So, MPS has a significantly higher spectral efficiency than these other techniques.

IV. CONCLUSION

We have described and demonstrated a MPS measurement setup capable of measuring DGD in a bandwidth of 4.92 GHz with a single-measurement expanded uncertainty of less than 40 fs for devices with DGD between 10 and 1000 fs and with larger uncertainties for values beyond 1000 fs. As the mean DGD grows, the uncertainty source is dominated by the linearity uncertainty of the system, which could be improved with better linearity calibrations. We also found that for smaller DGD values, polarization dependence in the polarization controller and detector can contribute significantly to the uncertainty, but the contribution can be reduced by multiple measurements with polarization randomized.

APPENDIX A
DETERMINING THE INTERNAL DGD

The inherent DGD of each element in the measurement path was determined in order to calculate its uncertainty contribution to the measurement. Following are a list of the elements contributing DGD to the measurement, and, where appropriate, a description of how this internal DGD was measured.

A. Fiber Leads

The fiber leads ("Lead 1" and "Lead 2" of Fig. 1) were measured using a Jones Matrix Eigenanalysis technique [5] and found to have about 0.8 fs of DGD each.

B. Polarization Controller

The DGD inherent in the polarization controller (PC2 of Fig. 1) likely comes from a couple of different sources. The most obvious one is due to the birefringence of the waveplates used to change the state of polarization. Our polarization controller is described schematically in Fig. 1, and consists of a bulk polarizer, quarter waveplate, and half waveplate. The waveplates used are zero-order, and so, at 1550 nm, the DGD of the quarter and half waveplates is about 1.3 fs and 2.6 fs, respectively. The contribution of these DGDs to the MPS measurement of the DUT is complicated in that the orientation of the waveplates changes for each of the six launched states. So we cannot treat the polarization controller as a fixed DGD element. Instead, for each of the six launch states, we find the waveplate-induced bias on the RF phase delay. We find that these six bias values (corresponding to the six launched polarization states) combine in a DGD measurement to look like a net 1.3 fs DGD for a simple $\boldsymbol{S}_1, -\boldsymbol{S}_1, \boldsymbol{S}_2, -\boldsymbol{S}_2, \boldsymbol{S}_3, -\boldsymbol{S}_3$ launch. This 1.3 fs bias may add to or subtract from the DGD of the DUT, depending on the relative orientation between PC2 and the DUT. However, to randomize this bias effect, we randomize the absolute orientation of the six-state set. This reduces the average DGD bias due to the DGD of the polarization controller. Of course, this complicates the calculation of bias DGD, because the effective DGD of the polarization controller is now a function of the orientation of the waveplates both with respect to each other and with respect to the input polarizer. We treat this extra complication by calculating the effective DGD of the polarization controller for all possible orientations the waveplates could assume in multiple measurements where the 6 state sets are launched with random overall orientation. Averaging these possible states gives an effective mean DGD error of 1.8 fs due to waveplate retardance.

It turns out that waveplate DGD is not all that contributes to the DGD in the polarization controller. Internal fiber-lead birefringence can also contribute. We measured the DGD of the polarization controller by placing it in the measurement path of a JME measurement system and found that the measured DGD for a variety of waveplate orientations varied from 2.5 fs to 5 fs.

A more subtle source of apparent DGD is due to what seems to be beam steering as the polarization optics are rotated. With the MPS system set up as in Fig. 1 (except with no DUT in place), the detected RF phase was measured as the half and quarter waveplates of the polarization controller (PC2) were stepped through all possible orientations. We found that waveplate orientations that differed by 180° did not always yield the same RF phase delay. One would expect that the polarization controller would present the same optical delay when one of its waveplates is oriented at an angle x as when the waveplate is oriented at $x + 180°$. However, we found one waveplate yielded as much as a 9 fs difference between the two orientations. We attribute this behavior to beam steering as the waveplate rotates. This beam steering doesn't appreciably affect the polarization properties, but does vary the optical delay through the device. This polarization-dependent optical path delay in the polarization controller can give apparent DGD in the MPS measurement, and it is not detectable when measuring the polarization controller's DGD with the JME system.

In order to assess the actual DGD contribution of the polarization controller to our MPS measurement, we used the MPS setup of Fig. 1 to measure the DGD of a stabilized DGD element of nominally 315 fs. We made 20 measurements of the DGD and averaged the results, then the fiber lead between the polarization controller and the DUT was moved and another set of measurements was made and averaged. This process was repeated 10 times and yielded a low noise measurement of the variation in measured DGD as the coupling between the polarization controller and the DUT was changed. We found a maximum variation with lead reorientation of ±9 fs. This variation can be attributed to the vector addition between the polarization controller's DGD and the DGD of the elements beyond the polarization controller. We expect that the maximum range of this variation is twice the DGD contribution of the polarization controller itself (since the largest differences in measured results will correspond to adding or subtracting the DGD of the polarization controller). Using this result, we assigned a 9 fs effective DGD to the polarization controller.

C. Detector

We were surprised to find that the detector contributes significantly to the internal DGD of the measurement system. We found the measured group delay at the detector depended on the orientation of the polarization state into the detector. This is likely a common occurrence, but it is not a problem in non-RF DGD measurements. In such DGD measurement systems as JME, interferometry, fixed analyzer (wavelength scanning), etc., the detector measures only the received optical intensity, which is then related to DGD. However, in RF phase-shift measurements, the direct output of the measurement system is RF phase delay as a function of optical polarization. So, a polarization-dependent group delay in the detector could look like a DGD.

We measured the magnitude of this polarization-dependent group delay in the detector in the same way as we assessed the DGD effects from the polarization controller. We used the MPS setup of Fig. 1 to measure the DGD of a stabilized DGD element of nominally 315 fs. Twenty measurements of the DGD were made and the results averaged, then the fiber lead between the DUT and the detector was moved and another set of measurements was made and averaged. This process was repeated 12

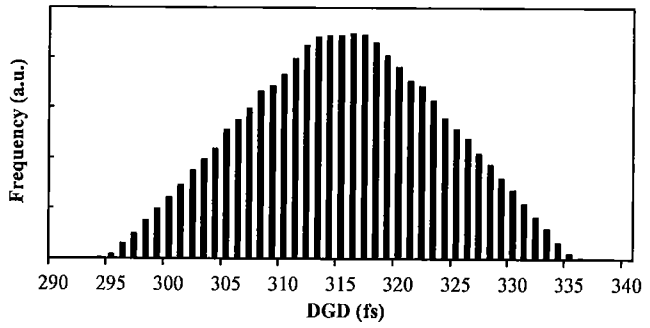

Fig. 5. Histogram of DGD obtained by simulation for five DGD elements in measurement path with values 9 fs, 0.8 fs, 315 fs, 0.8 fs, and 11 fs. The DGD distribution was generated by simulating randomized coupling between the elements.

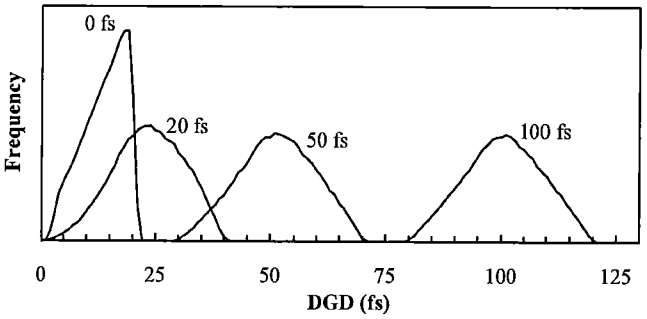

Fig. 6. Statistical distribution of measured DGD (assuming random lead reorientations) for various values of DGD in the DUT with elements of 9 and 0.8 fs before the DUT and 0.8 and 11 fs after the DUT.

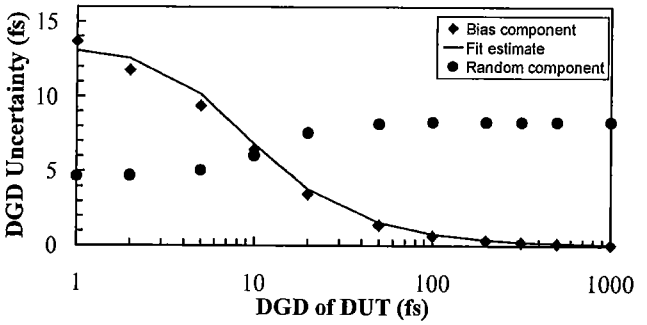

Fig. 7. Components of uncertainty due to internal DGD; curve generated using (B2).

times to give a low-noise measurement of the polarization-dependent group delay at the detector. We found a maximum variation in measured group delay of ±11 fs. This means the detector exhibits an effective DGD of 11 fs.

Appendix B
Mitigating Internal DGD Effects

Appendix A identifies four sources of internal DGD in the MPS measurement system. We minimize the measurement error due to these DGD sources by averaging multiple measurements made with randomized polarization coupling between DGD sources. In other words, between measurements, we reorient the fiber lead going from the polarization controller to the DUT and the fiber lead going from the DUT to the detector. We also randomize the absolute orientation of the six-polarization-state set that is launched. Moving the fiber leads and reorienting the launched states serves to randomize the polarization coupling between the DGD elements in the measurement path. PMD is a vector quantity, and so, the net DGD from a series of PMD elements is given as a vector sum. Using the concatenation rules of [12], we find that for five PMD elements in a row, the net polarization dispersion vector (PDV) Ω_{Tot} is a function of the individual PDVs and their rotation matrices, given by

$$\boldsymbol{\Omega_{Tot}} = \boldsymbol{\Omega_5} + \boldsymbol{R_5\Omega_4} + \boldsymbol{R_5R_4\Omega_3} + \boldsymbol{R_5R_4R_3\Omega_2} + \boldsymbol{R_5R_4R_3R_2\Omega_1} \tag{B1}$$

where $\boldsymbol{\Omega_i}$ is the PDV of the ith element, and $\boldsymbol{R_i}$ is the polarization transfer (rotation) matrix of the ith element. To calculate the effect on our measurements of randomly orienting the fiber leads, we average (B1) for all possible orientations of the various elements. We do this by assigning the measured DGD values for each element as the magnitude of the associated PDV. But the orientations of each PDV and its associated rotation matrix $\boldsymbol{R_i}$ are randomized. Fig. 5 shows the distribution of $\boldsymbol{\Omega_{Tot}}$ obtained for our MPS system for simulated measurements of a 315 fs DUT, (given the internal DGD sources mentioned, $|\boldsymbol{\Omega_1}| = 9$ fs, $|\boldsymbol{\Omega_2}| = 0.8$ fs, $|\boldsymbol{\Omega_3}| = 315$ fs, $|\boldsymbol{\Omega_4}| = 0.8$ fs, and $|\boldsymbol{\Omega_5}| = 11$ fs). This represents the expected distribution of DGD values to be measured when the DUT is 315 fs and the fiber leads are reoriented in between measurements. For 2×10^5 simulations, we found the expected mean DGD is 315.2 fs and the standard deviation 8.3 fs.

Of course, this distribution changes for different DGD values of the DUT. Fig. 6 shows DGD distributions obtained by simulation for a range of DGD values of the DUT (assuming the fiber leads are reoriented between measurements). Fig. 7 shows the predicted discrepancy between the mean of multiple DGD measurements (with the fiber leads reoriented each time) and the true DGD of the DUT. We call this the "bias component" and denote it as $\Delta\tau_{\mathrm{Int}}$. The predicted standard deviation of multiple measurements is also given in Fig. 7. We call this the "random component", and denote it σ_{Int}. For simplicity, we estimate an empirical fit to the bias data and find that within about 1 fs it behaves as

$$\Delta\tau_{\mathrm{Int}} \approx 79.4 \frac{1}{\sqrt{\Delta\tau_{\mathrm{DUT}}^2 + 36}} \tag{B2}$$

where $\Delta\tau_{\mathrm{DUT}}$ is the true DGD of the DUT, and the units of $\Delta\tau_{\mathrm{DUT}}$ and $\Delta\tau_{\mathrm{Int}}$ are femtoseconds. The 36 fs^2 value in (B2) was added empirically to describe the dominance of internal DGD at low values (<10 fs) of $\Delta\tau_{\mathrm{DUT}}$. This happens because DGD is the magnitude of a vector quantity (the PDV). So, random noise vectors such as internal DGD will only yield a zero mean when their values are sufficiently lower than the DUT DGD. In certain cases, this effect can be mitigated by calculating the DUT DGD as the magnitude of the vector average of the PDV values obtained with the multiple measurements (rather than as the average of the magnitude of the various PDVs). This vector average approach requires that all directional changes of the PDV are due to noise and so requires that the DUT be non-mode-coupled.

If we are to make multiple measurements and average the results, it is important to know how the standard deviation of the mean (SDOM) scales with multiple measurements. As shown in Fig. 6, the shape of the distribution of the measured DGD depends on the DGD of the DUT. However, through simulation, we find that for the DUT DGD values we simulated (0 to 1000 fs), the SDOM scales approximately as $N^{-1/2}$, where N is the number of independent measurements (made with the fiber leads reoriented).

APPENDIX C
SPECTRAL EFFICIENCY

In all methods of DGD measurement, there is a tradeoff between the spectral bandwidth used to make the measurement and the achievable DGD resolution. The bandwidth efficiency factor α_{BEF} relates the DGD-bandwidth product to the achievable SNR as

$$\alpha_{\mathrm{BEF}} = \left(\frac{\mathrm{SNR}}{\Delta\omega}\right)\frac{1}{\Delta\tau} \tag{C1}$$

where $\Delta\tau$ is the DGD of the device and $\Delta\omega$ is the angular frequency spectrum used by the measurement [11]. α_{BEF} can be thought of as the achievable SNR per bandwidth normalized to the mean DGD. Equation (C1) illustrates that for a given measurement, the SNR can be improved by increasing the measurement bandwidth. Or, when the measurement bandwidth is fixed, the SNR improves when measuring larger DGDs. α_{BEF} is dependent on the particular measurement technique and the quality of the equipment. Expressing SNR as $\Delta\tau/\sigma$, where σ is the measurement standard deviation, we can write the efficiency as

$$\alpha_{\mathrm{BEF}} = \frac{1}{\sigma\cdot\Delta\omega}. \tag{C2}$$

This useful form makes calculation of α_{BEF} simple. For our measurement technique, we demonstrated a standard deviation below 9 fs for the 315 fs device. This gives a bandwidth efficiency factor of 3600 (using $2\cdot 2\pi\cdot 2.46\times 10^9$ Hz for $\Delta\omega$). Of course, α_{BEF} addresses random uncertainty and its change with measurement bandwidth, and should not be confused with the full (expanded) uncertainty of the measurement.

Spectral efficiencies are often difficult to estimate from the literature because spectral and temporal uncertainty are rarely specified together. A technical specification sheet from a particular swept-wavelength interferometer specifies a 27 fs noise uncertainty in 50 pm bandwidth and a 85 fs noise uncertainty in a 10 fs bandwidth (each with 30 averages). This yields α_{BEF} values from 950 to 1500. The fact that the efficiency appears to change with spectral resolution indicates the presence of a noise floor, independent of bandwidth. JME measurement results supplied to us informally show standard deviation of the DGD for a single measurement of about 67 fs in a 25-pm bandwidth, giving a α_{BEF} value of ~800. These spectral efficiency values are included only for a rough comparison and do not necessarily represent the state of the art of these other techniques.

REFERENCES

[1] P. A. Williams, "Modulation phase-shift measurement of PMD using only four launched polarization states: a new algorithm," *Electron. Lett.*, vol. 35, pp. 1578–1579, 1999.

[2] L. E. Nelson, R. M. Jopson, H. Kogelnik, and J. P. Gordon, "Measurement of polarization mode dispersion vectors using the polarization-dependent signal delay method," *Opt. Express*, vol. 6, pp. 158–167, 2000.

[3] G. D. VanWiggeren, A. R. Motamedi, and D. M. Baney, "Single-scan interferometric component analyzer," *IEEE Photon. Technol. Lett.*, vol. 15, pp. 263–265, 2003.

[4] A. J. Barlow, J. Henstock, and C. Mackechnie, "Modulation phase shift measurement of PMD: toward and engineered solution," in *Tech. Dig.—Symp. Optical Fiber Measurement*, Boulder, CO, 2000, pp. 83–86.

[5] P. A. Williams, "Rotating-wave-plate Stokes polarimeter for differential group delay measurements of polarization mode dispersion," *Appl. Opt.*, vol. 38, pp. 6508–6515, 1999.

[6] H. Goldstein, *Classical Mechanics*, 2nd ed. Reading, MA: Addison-Wesley, 1980, pp. 143–148.

[7] N. Cyr, M. Leclerc, and B. Ruchet, "PMD measurements in multipath components: the single waveplate example," in *Proc. Photon. North*, Quebec, Canada, 2002.

[8] P. A. Williams and J. D. Kofler, "Measurement and mitigation of multiple reflection effects on the differential group delay spectrum of optical components," in *Tech. Dig.—Symp. Optical Fiber Measurement*, Boulder, CO, 2002, pp. 173–176.

[9] Guidelines for Evaluating and Expressing the Uncertainty of NIST Measurement Results, B. N. Taylor and C. E. Kuyatt, Eds., National Inst. Stand. Technol., 1994.

[10] P. A. Williams, S. M. Etzel, J. D. Kofler, and C.-M. Wang, Standard Reference Material 2538 for Polarization-Mode Dispersion (Non-Mode-Coupled), NIST Special Publication 260-145, 2002.

[11] P. A. Williams, "PMD measurement techniques—avoiding measurement pitfalls," in *Venice Summer School on Polarization Mode Dispersion*, Venice, Italy, June 24–26, 2002.

[12] J. P. Gordon and H. Kogelnik, "PMD fundamentals: polarization mode dispersion in optical fibers," in *Proc. National Acad. Sci.*, vol. 97, 2000, pp. 4541–4550.

P. A. Williams received the Ph.D. degree in physics from the University of Colorado at Boulder in 1993.

Since 1988, he has been with the National Institute of Standards and Technology (NIST), Boulder, CO, working in the fields of ferroelectric liquid crystals, polarization, optical fiber, and polarization-mode dispersion.

J. D. Kofler received the B.S. degree in physics from the University of California at Davis in 1987 and the M.S. degree in physics from the University of Colorado at Boulder in 1989.

Since 2001, he has been with the National Institute of Standards in Technology (NIST), Boulder, CO, specializing in polarization-mode dispersion.